Available online at www.sciencedirect.com
ScienceDirect
Trans. Nonferrous Met. Soc. China 33(2023) 2168−2182
Transactions of Nonferrous Metals Society of China
www.tnmsc.cn

Linear energy storage and dissipation laws and damage evolution characteristics of rock under triaxial cyclic compression with different confining pressures

Song LUO[1], Feng-qiang GONG[1,2], Liu-liu LI[1], Kang PENG[1]

1. School of Resources and Safety Engineering, Central South University, Changsha 410083, China;
2. School of Civil Engineering, Southeast University, Nanjing 211189, China

Received 17 March 2022; accepted 22 June 2022

Abstract: Triaxial cyclic compression tests with different confining pressures were conducted to explore the energy distribution characteristics of rock and their responses to confining pressure. The pre-peak input strain energy, pre-peak elastic strain energy, and pre-peak dissipated strain energy at different stress levels were computed based on the resultant stress−strain curves. The results indicated that under different confining pressures, both the pre-peak elastic strain energy and pre-peak dissipated strain energy were linearly related to the pre-peak input strain energy, and thus the linear energy storage and dissipation laws in triaxial cyclic compression were confirmed. The energy storage coefficient in triaxial compression of the rock was positively correlated with the confining pressure, whereas the corresponding energy dissipation coefficient exhibited an opposite correlation. Using the linear energy storage law, the peak elastic strain energy and peak dissipated strain energy of rock in triaxial compression were deduced. Furthermore, the damage evolution characteristics of rock under different confining pressures were analysed by considering the linear energy dissipation law.

Key words: energy distribution law; energy storage; energy dissipation; triaxial compression; cyclic loading; confining pressure

1 Introduction

The deformation and failure in rocks are essentially structural adjustment progresses driven by energy conversion and transfer. The use of energy theory follows the nature of rock failure, and can deepen the understanding of rock failure phenomena, thus bringing new perspectives and solutions for related deep rock engineering problems [1−3]. For example, extensive theoretical and experimental efforts have confirmed that it is useful to understand rock failure phenomena from the energy theory, such as the rockburst during deep mining or tunneling projects [4−8].

Regarding the energy behavior during rock failure, many valuable results have been achieved by means of laboratory experiments [9−14]. For examples, LI et al [15] conducted the triaxial compression tests on different types of rocks and modified a brittleness index considering energy dissipation. ZHANG et al [16,17] analyzed the fracturing behaviors of hard rocks under true triaxial stress using energy principles, and concluded that strain energy analysis method can effectively explain the macroscopic and microscopic failures of rocks. The influence of loading rate and unloading rate on rock strain energy in true triaxial compression was also studied by ZHAO et al [18], who found that as the loading rate

Corresponding author: Feng-qiang GONG, E-mail: fengqiangg@126.com; Kang PENG, E-mail: pengkang2020@csu.edu.cn
DOI: 10.1016/S1003-6326(23)66251-X
1003-6326/© 2023 The Nonferrous Metals Society of China. Published by Elsevier Ltd & Science Press

increased, the total strain energy, elastic strain energy, and dissipated strain energy increased. GAO and YANG [19] investigated the role of strain energy in rockburst in terms of experimental and numerical methods through composite rock−coal specimens and offered the evidence that the elastic strain energy accumulated in rocks was converted into the kinetic energy and was released during rockburst. XIAO et al [20] established an energy calculation equation in consideration of the confining pressure and seepage pressure via cyclic loading−unloading tests. Using the elastic to dissipated energy ratio and elastic to total energy ratio, KHAN et al [21] predicted the early failure point of rock containing different water contents, and provided an effective method for monitoring the disasters that may occur in underground projects.

The above efforts greatly contribute to the development and application of energy theory in rock mechanics problems. However, the distribution law of strain energy and how the input strain energy is allocated into elastic strain energy and dissipated strain energy during rock loading has less been studied. To achieve favorable results and make the application of energy interpretations more scientific and extensive in related rock engineering, it is necessary to first understand the law of energy distribution clearly in rock under different stress states [22,23]. In previous studies, GONG et al [24,25] have first revealed the linear energy storage (LES) law and linear energy dissipation (LED) law of rocks in uniaxial stress conditions and confirmed that these linear energy laws always appeared despite the loading forms and rock failure modes [26]. Upon the LES law, they modified and improved several classic rockburst proneness indexes [24,27]. However, the LES and LED laws have not been investigated in triaxial stress conditions and the coupling effect of confinement and cyclic loading has not been studied. During construction of deep engineering projects, surrounding rocks are inevitably subjected to confinement effect and cyclic loads caused by external influences such as chamber excavation, blasting, and geological tectonic movement [28−34]. Cyclic compression is an applicable approach for measuring the deformation and damage behavior of rocks [35−38]. Thus, studying the energy mechanism under triaxial cyclic loading is of practical significance to deep rock engineering problems.

In this study, several groups of triaxial cyclic compression tests were conducted on MTS 815 testing system to investigate the energy distribution laws of red sandstone. Based on the experimental results, the existence of LES and LED laws in triaxial cyclic compression was confirmed, and the effect of confining pressure on the energy distribution laws was analyzed. Subsequently, the universality of the LES and LED laws under triaxial stress states was carefully tested by extracting the experimental data in literature. Further, using the LED law, the damage evolution process of rock in triaxial compression with different confining pressures was characterized.

2 Experimental

2.1 Specimen preparation

The red sandstone sampling from Linyi City, Shandong Province, China, was used as the testing material. Rock specimens were processed into cylinders with a height of 100 mm and a diameter of 50 mm using a rock cutting machine. The end faces of rock specimens were polished to ensure that their unevenness is less than 0.1 mm, and that the vertical angle error between the specimen axis and end face is no more than 0.25°. The mean density and P-wave velocity of the red sandstone are 2500 kg/m^3 and 3200 m/s, respectively. The uniaxial compressive strength of the red sandstone is approximately 98 MPa [24].

2.2 Testing apparatus and scheme

The MTS 815 testing system was used to perform the triaxial cyclic compression test with confining pressures of 5, 10, and 15 MPa. The testing system is mainly composed of the triaxial chamber, the water and oil hydraulic pumps, the electro-hydraulic servo control system, and the data display screen. The axial force of the test machine can reach 2600 kN with a measurement accuracy of ±0.5%. During experiments, the axial deformation of rock specimen was measured by an extensometer mounting on the specimen surface.

Figure 1 shows the stress path in a triaxial cyclic compression test. The detailed testing procedure is as follows:

(1) Triaxial compressive strength (TCS, σ_T) of

the red sandstone under three pre-set confining pressures (σ_3=5, 10, and 15 MPa) was first estimated. According to the obtained TCS under each confining pressure, five unloading stresses (σ_i) were predetermined in terms of $\sigma_i=i(\sigma_T-\sigma_3)+\sigma_3$ (wherein the stress level i was presupposed as 0.1, 0.3, 0.5, 0.7, and 0.9).

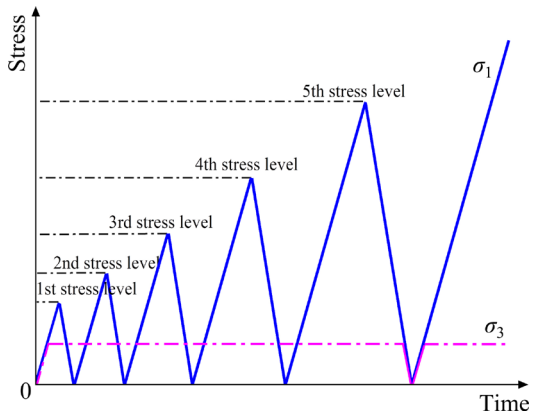

Fig. 1 Schematic curve of stress path in triaxial cyclic compression test

(2) For the triaxial cyclic compression test, axial and circumferential stresses were first applied simultaneously to the pre-set confining pressure (e.g., 5 MPa) at a rate of 0.1 MPa/s. Keeping the confining pressure constant, the axial stress was increased to the first stress level at the rate of 0.1 MPa/s, and then decreased to approximate 0 at the same rate of loading to complete the first cycle. Following the four remaining stress levels involved in Step (1), similarly repeat the four related cycles until the fifth cycle. In the fifth cycle, the axial stress was firstly decreased to the value of confining pressure, and then the axial stress and the confining pressure were simultaneously released to about 0 at a rate of 0.1 MPa/s, completing the fifth cycle.

(3) Finally, the axial and circumferential stresses were simultaneously applied to the value of pre-set confining pressure at the rate of 0.1 MPa/s. Keeping the confining pressure unchanged, the rock specimen was axially compressed to failure at the rate of 0.1 mm/min. The force-controlled mode was switched to displacement-controlled mode during loading to prevent sudden instability of rock specimens after peak stress from causing damage to the testing machine. According to the triaxial peak stress (TPS, σ_P) obtained in this triaxial cyclic compression test, the actual stress level (i_c) is determined as

$$i_c=[i(\sigma_T-\sigma_3)+\sigma_3]/(\sigma_P-\sigma_3) \quad (1)$$

2.3 Energy theory for rock triaxial cyclic compression test

In the triaxial compression test, because the circumferential strain energy is small and it not directly damages or destabilizes the rock specimen, the impact of circumferential strain energy on test results can be ignored to a certain extent [2,39−41]. Further, the aim of this study is to explore the distribution laws of energy storage and dissipation under cyclic loading and their responses to confining pressure. As a result, herein we only focus on the energy characteristics in the axial loading direction of rock specimens. If no heat exchange exits between the specimen loading system and the outside environment, strain energies including the pre-peak input strain energy U_i^I, pre-peak elastic strain energy U_i^e and pre-peak dissipated strain energy U_i^d at stress level i can be determined by the following formulas according to the first law of thermodynamics [1], as shown in Fig. 2.

$$U_i^I=\int_{\varepsilon_{i-1}^p}^{\varepsilon_i^u}(\sigma_1-\sigma_3)\mathrm{d}\varepsilon_1 \quad (2)$$

$$U_i^e=\int_{\varepsilon_i^p}^{\varepsilon_i^u}(\sigma_1-\sigma_3)\mathrm{d}\varepsilon_1 \quad (3)$$

$$U_i^d=U_i^I-U_i^e \quad (4)$$

where ε_i^p and ε_i^u separately denote the permanent strain and the total strain corresponding to stress level i, and ε_{i-1}^p refers to the permanent strain produced in the last loading−unloading cycle.

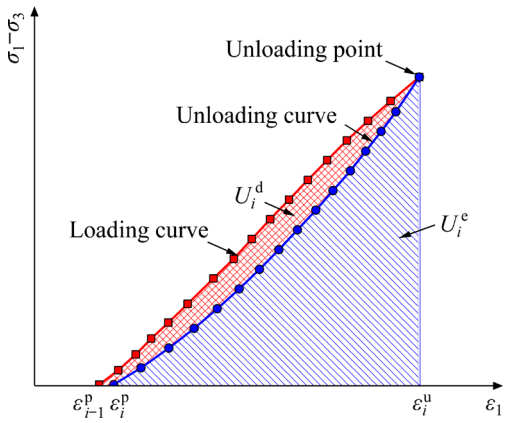

Fig. 2 Schematic curve of strain energies in triaxial cyclic compression at stress level i

3 Results and analysis

3.1 Mechanical characteristics

3.1.1 Stress−strain curves

Figure 3 shows the representative axial stress−strain curves in the triaxial cyclic compression tests. It is obvious that a higher confining pressure leads to the greater peak strength and peak strain. The post stress−strain curve behaves gentler under a higher confining pressure,

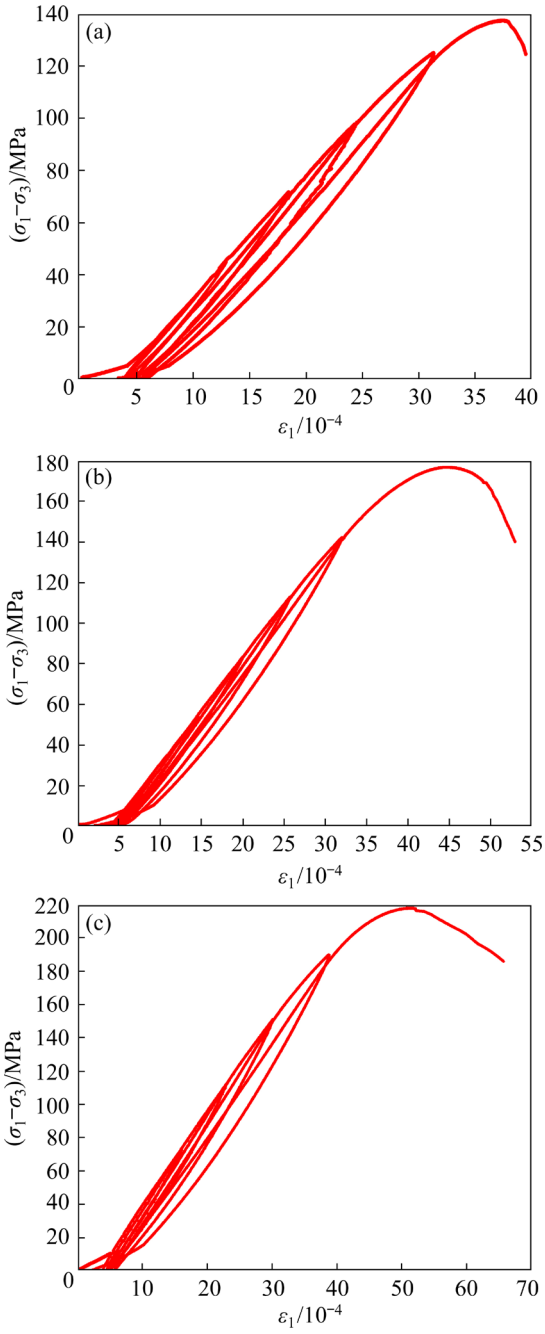

Fig. 3 Axial stress−strain curves of rock specimens in triaxial cyclic compression tests with different confining pressures: (a) 5 MPa; (b) 10 MPa; (c) 15 MPa

indicating an improvement of rock plasticity due to confinement. It is also observed that the subsequent loading curve always passes through the intersection of the last loading and unloading curves, and continues to develop along the previous loading path. This observation implies that the rock has a memory of the initial loading path in a triaxial compression state. When the axial stress is approximately zero, the end of an unloading curve does not return to the starting point of the original loading curve. This phenomenon indicates that the rock has undergone irreversible deformation under cyclic stress, i.e., the plastic deformation. The plastic deformation consumes part of the input strain energy of the rock specimen. With increasing stress level, the proportion of strain energy dissipated in rock increases. Therefore, the end of the unloading curve is farther and farther away from the starting point of the initial loading curve.

3.1.2 Characteristics of elastic strain and plastic strain under various stress levels

Figure 4(a) illustrates the variation trend of axial elastic strain ($\varepsilon_i^{\mathrm{u}}-\varepsilon_i^{\mathrm{p}}$) versus the actual stress level in the triaxial cyclic compression test. It is found that the axial elastic strain increases with the actual stress level in highly linear relations. The coefficient of determination R^2 resulted from the regression analysis is greater than 0.9950, indicating a strong correlation between the two parameters. Interestingly, under different confining pressures, at a similar actual stress level greater than 0.3 approximately, the higher the confining pressure is, the greater the elastic strain is. With an increase in actual stress level, the difference between axial elastic strains under various confining pressures becomes greater. However, it seems that the elastic strain under 10 MPa is the greatest when the actual stress level is less than 0.3. At low actual stress level, the difference between elastic strains under three confining pressures is small. Overall, a higher confining pressure causes a greater elastic strain. This is because with an increase in confining pressure, the strength of rock specimen increases. Since the number of cycles in the triaxial cyclic compression test is constant, the loading−unloading gradient increases, which determines that the elastic deformation increases with the confining pressure.

Figure 4(b) depicts the variation trend of axial plastic strain ($\varepsilon_i^{\mathrm{p}}-\varepsilon_{i-1}^{\mathrm{p}}$) with respect to the actual

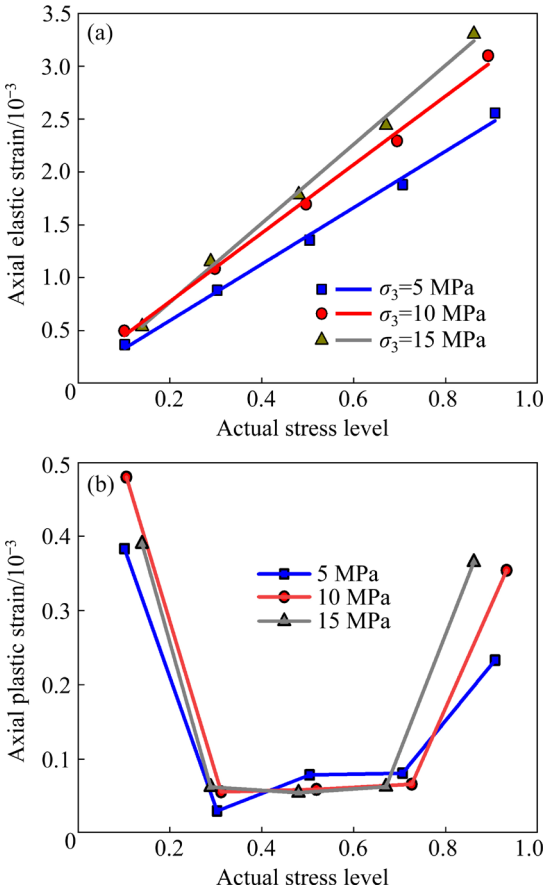

Fig. 4 Correlations between axial elastic strain (a), axial plastic strain (b), and actual stress level under different confining pressures

stress level under different confining pressures. Obviously, a "U"-shaped variation trend is presented. Since the energy dissipated during compression is mainly used for plastic deformation of the rock specimen, the change in plastic strain can be correlated with the dissipated strain energy during rock deformation. It is found that the plastic strain of the rock specimen is large in the first loading−unloading cycle. The main reason is that the rock specimen is initially compressed in the first cycle. At this time, its inner micro-cracks are initially compacted with an energy consumption, which is the so-called rock compaction stage. When the rock specimen undergoes the second, third, and fourth loading−unloading cycles, the plastic strain becomes less, and the less proportion of energy is consumed in these cycles than that in the first loading−unloading cycle. This is because after the first loading−unloading cycle, existing micro-cracks inside the rock specimen have already been compacted, and only the development of newly-generated cracks needs to consume energy. When the rock specimen suffers from the fifth cycle, the plastic strain increases suddenly. In this case, massive cracks begin to develop and extend, and the rock specimen is about to failure.

3.2 Nonlinear variation pattern of pre-peak strain energy in triaxial cyclic compression

According to Eqs. (2)−(4), the U_i^{I}, U_i^{e}, and U_i^{d} were computed. The relations between these three pre-peak strain energies and the actual stress level under distinct confining pressures are plotted. As shown in Fig. 5, under all confining pressures,

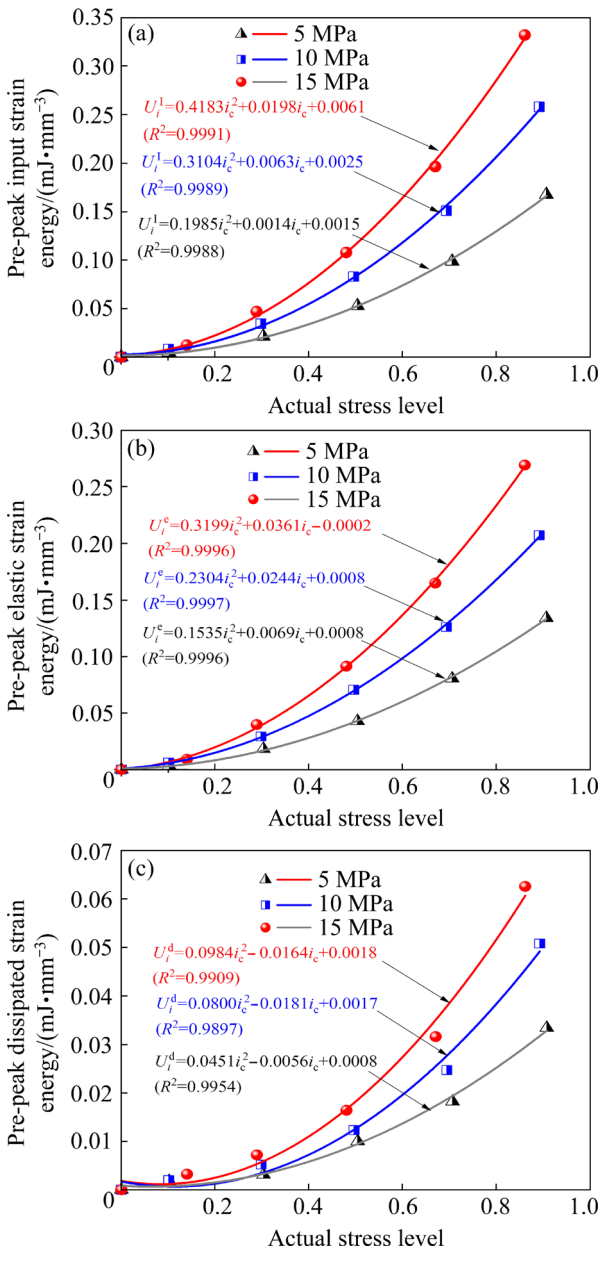

Fig. 5 Growth trends of three pre-peak strain energies of red sandstone under different actual stress levels and confining pressures: (a) U_i^{I}; (b) U_i^{e}; (c) U_i^{d}

the U_i^{I}, U_i^{e}, and U_i^{d} present a similar nonlinear growth with the actual stress level. The growth trend can be described using quadratic functions, whose R^2 values all exceed 0.98. In addition, under approximately the same actual stress level, each type of pre-peak strain energy also increases with the confining pressure. When the confining pressure increases from 5 to 15 MPa, the U_i^{e} is increased by 2.4 times (Fig. 5(b)), while the U_i^{d} is only increased by 1.6 times (Fig. 5(c)). For example, when the actual stress level is approximately 0.8, the U_i^{e} and U_i^{d} under 5 MPa confining pressure are about 0.1 and 0.03 mJ/mm^3, and those of specimens under 10 MPa confining pressure are approximately 0.16 and 0.035 mJ/mm^3, respectively. Under the confining pressure of 15 MPa, the U_i^{e} is about 0.24 mJ/mm^3, and the U_i^{d} is about 0.05 mJ/mm^3. The analysis above indicates that increasing the confining pressure is beneficial to the conversion of U_i^{I} into U_i^{e} inside the rock, thus meanwhile restraining the performance of energy dissipation.

3.3 Relationships of three pre-peak strain energies in triaxial cyclic compression

Figure 6 illustrates the mutual relationships between the three pre-peak strain energies under different confining pressures. It is found that as U_i^{I} increases, both U_i^{e} and U_i^{d} increase linearly, with the R^2 exceeding 0.97. It should be noted that to rectify a deviation, the coordinate origin (0,0) was included during data regression [25]. These preliminary linear relations are expressed by Eq. (5):

$$\begin{cases} U_i^{\mathrm{e}} = a_{\mathrm{T}} U_i^{\mathrm{I}} + b_{\mathrm{T}} \\ U_i^{\mathrm{d}} = c_{\mathrm{T}} U_i^{\mathrm{I}} - b_{\mathrm{T}} \\ c_{\mathrm{T}} = 1 - a_{\mathrm{T}} \end{cases} \tag{5}$$

In the above formulas, to quantitatively describe the energy storage and dissipation performances during triaxial cyclic compression, a_{T} is defined as the energy storage coefficient (ESC) and c_{T} as the energy dissipation coefficient (EDC) in triaxial compression. b_{T} is caused by the rock

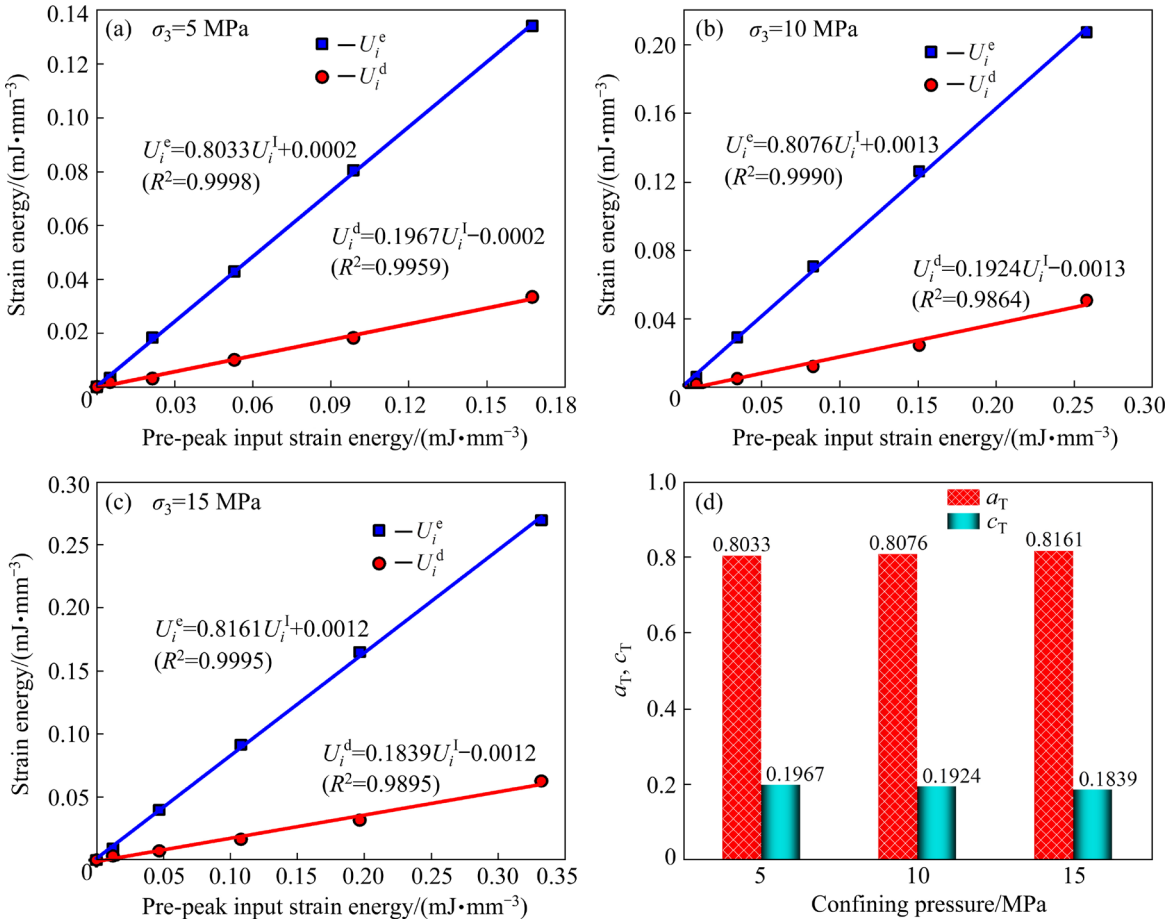

Fig. 6 Linear relationships between three strain energies of red sandstone (RS) in triaxial cyclic compression test: (a) σ_3=5 MPa; (b) σ_3=10 MPa; (c) σ_3=15 MPa; (d) a_{T}, c_{T}

heterogeneity and discrete energy data of rock specimens and is very small relative to a_T or c_T, which is ignorable in some cases. Therefore, Eq. (5) can essentially be replaced by Eq. (6). This also indicates that the U_i^I is proportionally distributed into U_i^e and U_i^d in the process of triaxial compression. The proportional relationship between U_i^e and U_i^I is termed as the LES law, and that between the U_i^d and U_i^I as the LED law. As a result, the ESC and EDC in triaxial cyclic compression can be determined by Eq. (7). As shown in Fig. 6, under the confining pressures of 5, 10 and 15 MPa, the value of ESC in triaxial compression follows an increasing order of 0.8033<0.8076<0.8161, and that of EDC shows the decreasing order of 0.1967>0.1924>0.1839 (Fig. 6(d)). When the confining pressure changes from 5 to 15 MPa, the ESC is increased by 1.59%, and the related EDC is reduced by 6.51%.

$$\begin{cases} U_i^e = a_T U_i^I \\ U_i^d = c_T U_i^I \\ c_T = 1 - a_T \end{cases} \tag{6}$$

$$\begin{cases} a_T = U_i^e / U_i^I \\ c_T = U_i^d / U_i^I \end{cases} \tag{7}$$

3.4 Universality of LES and LED laws in triaxial cyclic compression

As analysed earlier, the LES and LED laws were confirmed for the red sandstone during triaxial cyclic compression tests. To verify the generality of the LES and LED laws in such stress conditions, we extracted several sets of energy data from the stress−strain curves or related plots in the existing literature, wherein two types of sandstone [39,40], a type of limestone [42], and a type of marble [43], were tested under various confining pressures. Via linear regression analysis, we also found the linear energy storage and dissipation laws of the four types of rocks, as shown in Fig. 7 and Table 1. Despite of the variations in confining pressure, cycle number (or the number of stress level), and rock types, excellent mutual linear energy relations were confirmed, with the minimal R^2 greater than 0.96. This confirmation implies that the LES and

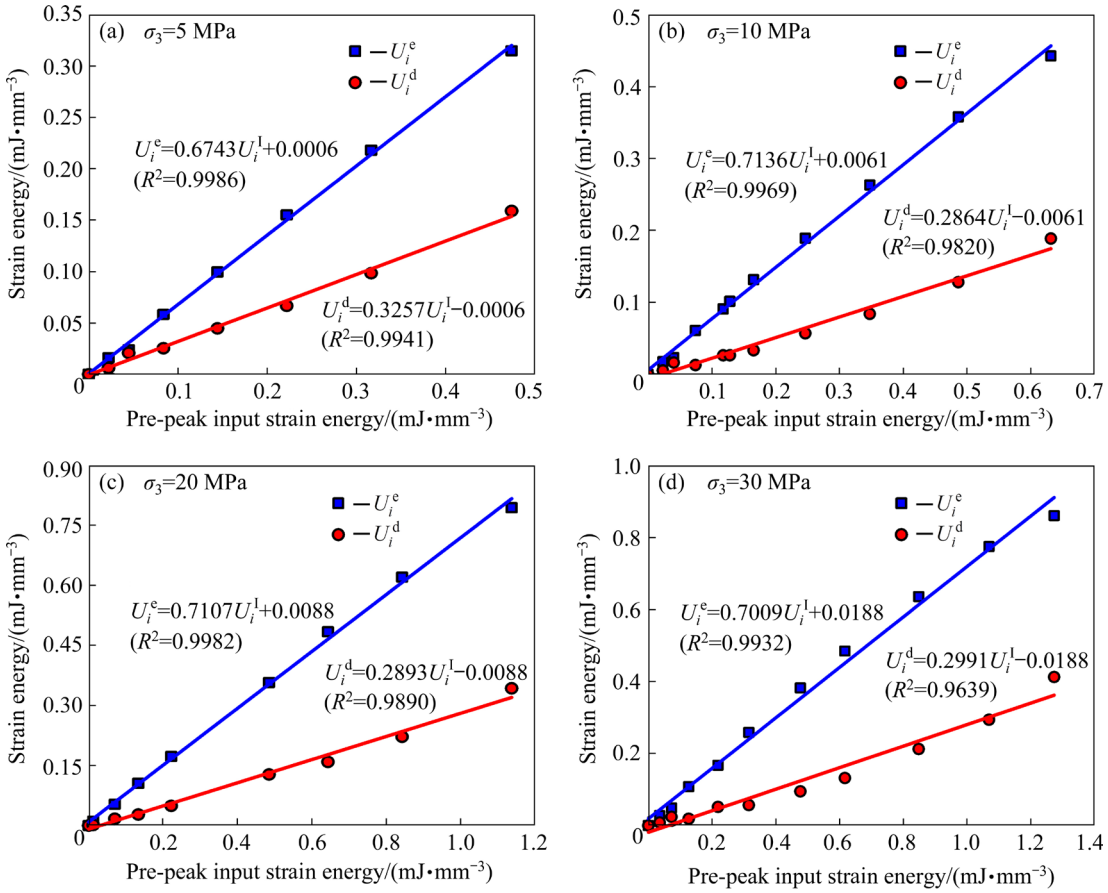

Fig. 7 LES and LED laws of Sandstone I (SI) under different confining pressures: (a) σ_3=5 MPa; (b) σ_3=10 MPa; (c) σ_3=20 MPa; (d) σ_3=30 MPa

Table 1 LES and LED laws of other three rocks under different confining pressures

Rock type	Confining pressure/ MPa	Linear energy relations	R^2
Limestone (LS)	1	$U_i^e=0.5839U_i^I+0.0012$	0.9866
		$U_i^d=0.4161U_i^I-0.0012$	0.9739
	5	$U_i^e=0.5879U_i^I+0.0025$	0.9938
		$U_i^d=0.4121U_i^I-0.0025$	0.9875
	10	$U_i^e=0.6079U_i^I+0.0046$	0.9903
		$U_i^d=0.3921U_i^I-0.0046$	0.9780
	15	$U_i^e=0.6473U_i^I+0.0039$	0.9903
		$U_i^d=0.3527U_i^I-0.0039$	0.9680
	20	$U_i^e=0.6559U_i^I+0.0070$	0.9967
		$U_i^d=0.3441U_i^I-0.0070$	0.9883
	25	$U_i^e=0.7172U_i^I+0.0036$	0.9991
		$U_i^d=0.2828U_i^I-0.0036$	0.9939
Sandstone II (SII)	5	$U_i^e=0.5922U_i^I+0.0024$	0.9946
		$U_i^d=0.4078U_i^I-0.0024$	0.9888
	10	$U_i^e=0.6326U_i^I+0.0008$	0.9982
		$U_i^d=0.3674U_i^I-0.0008$	0.9979
	20	$U_i^e=0.6636U_i^I-0.0044$	0.9981
		$U_i^d=0.3364U_i^I+0.0044$	0.9921
	30	$U_i^e=0.7100U_i^I+0.0212$	0.9958
		$U_i^d=0.2900U_i^I-0.0212$	0.9752
Crystalline marble (CM)	2.5	$U_i^e=0.5292U_i^I+0.0021$	0.9840
		$U_i^d=0.4708U_i^I-0.0021$	0.9798
	5	$U_i^e=0.4033U_i^I+0.0039$	0.9701
		$U_i^d=0.5967U_i^I-0.0039$	0.9861
	7.5	$U_i^e=0.4067U_i^I+0.0042$	0.9804
		$U_i^d=0.5933U_i^I-0.0042$	0.9907
	10	$U_i^e=0.4406U_i^I+0.0055$	0.9807
		$U_i^d=0.5594U_i^I-0.0055$	0.9880

LED laws are universal in rocks under triaxial cyclic stress conditions from two aspects. (1) The presence of LES and LED laws are unrelated to the rock type in triaxial cyclic compression. In this study, five types of rocks were involved, and they all obey the LES and LED laws, even though the specific linear regression of energy results seems quite difference for varied rock types. (2) The change of confining pressure also does not hinder the presence of LES and LED laws. It is clear that for each rock material subject to different confining pressures, the LES and LED laws are also captured. Therefore, it is rational to consider that the existence of the revealed LES and LED laws is of favourable universalism for rock in triaxial cyclic compression.

3.5 Variations in ESC and EDC with respect to confining pressure

Figure 8 presents the variations in the ESC and EDC of the above five rock types in triaxial cyclic compression with different confining pressures. Generally, it turns out that the ESC increases and EDC decreases with increasing confining pressure. In other words, a higher confining pressure normally causes a greater ESC and a smaller EDC. However, the influencing degree of confining pressure on these two coefficients differs due to the change of rock type. Compared with the two energy coefficients of other three rock types (RS, SI, CM in Figs. 8(a, b, e), those of the LS and SII (Figs. 8(c, d) are more sensitive to the variation of confining pressure. It is worth clarifying that a few cases exist, in which the ESC under a lower confining pressure is larger than that under a higher confining pressure. More specifically, the ESC of SI (Fig. 8(b)) under 10 MPa confining pressure is slightly greater than that under 20 and 30 MPa confining pressures. Similarly, for the CM (Fig. 8(e)), compared with the ESC resulted from the confining pressures of 5, 7.5, and 10 MPa, the ESC induced by 2.5 MPa confining pressure is greater. These cases may be caused by the discrepancy between physical properties of the same rock type under different confining pressures. However, it is still believed that the confining pressure plays a role in increasing the ESC. This can be confirmed by the fact that when confining pressure varies from 5 to 10 MPa, the ESC of CM increases and the corresponding EDC decreases (Fig. 8(e)). Also, the ESC of SI under 5 MPa confining pressure is smaller than that under the confining pressures of 10, 20, and 30 MPa (Fig. 8(b)). For the EDC of all rock types, opposite responses to the confining pressure were observed compared with the associated ESC. These findings indicate that increasing the confining pressure is

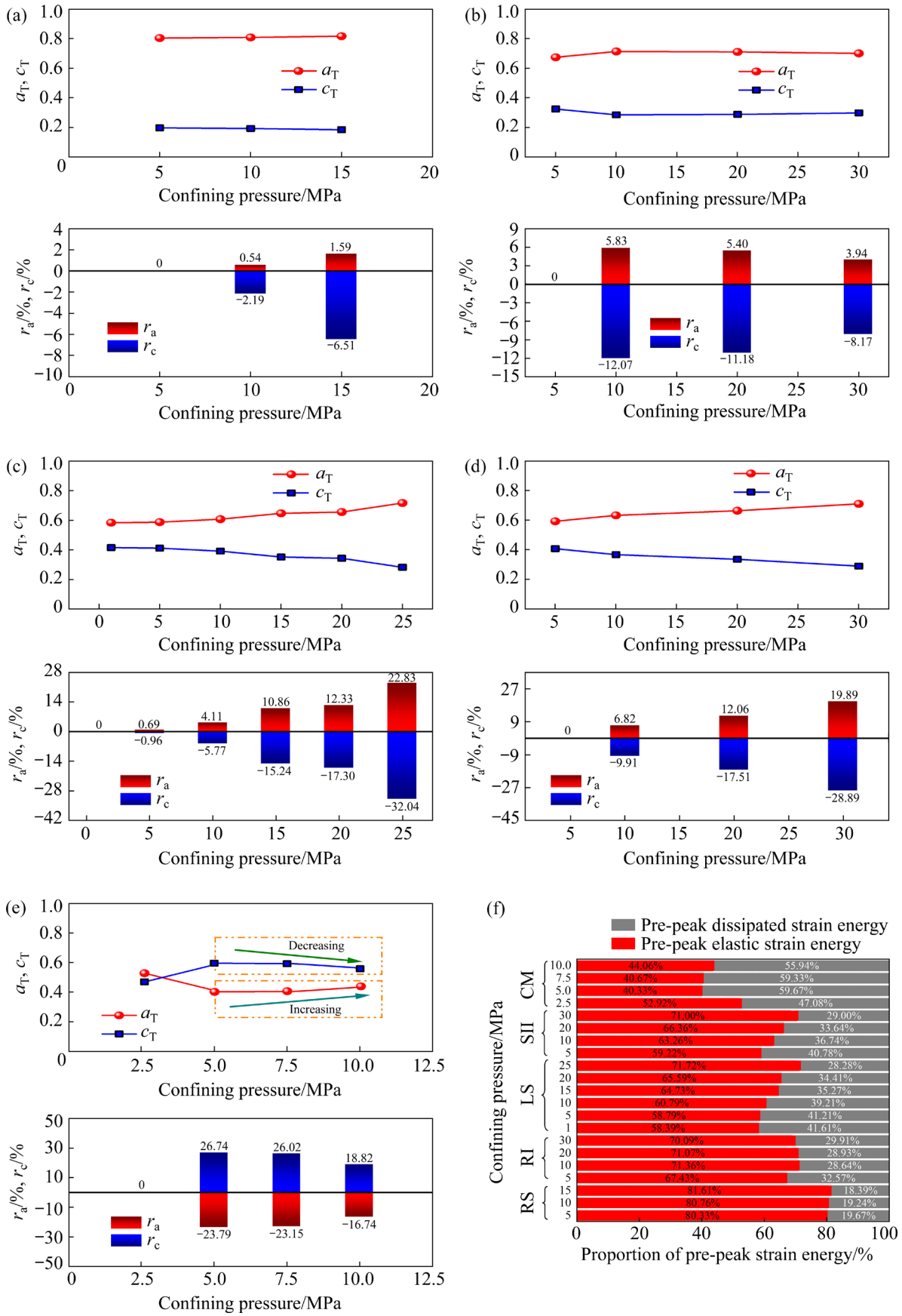

Fig. 8 ESC and EDC of different rocks subject to triaxial cyclic compression with various confining pressures: (a) RS; (b) SI; (c) LS; (d) SII; (e) CM; (f) Proportions of pre-peak strain energies

conducive to promoting the energy storage performance of rocks. Although in a few cases, the ESC under a lower confining pressure is slightly greater than that under a higher confining pressure, this does not affect the overall law that confining pressure promotes the energy storage capacity of rocks.

To further describe the influencing degree of confining pressure on these two energy coefficients through a quantitative manner, the variation rates of the two coefficients are determined as

$$\begin{cases} r_{\mathrm{a}} = \dfrac{a_{\mathrm{T}} - a_{\mathrm{T}}^{\min}}{a_{\mathrm{T}}^{\min}} \times 100\% \\ r_{\mathrm{c}} = \dfrac{c_{\mathrm{T}} - c_{\mathrm{T}}^{\min}}{c_{\mathrm{T}}^{\min}} \times 100\% \end{cases} \tag{8}$$

where r_{a} and r_{c} denote the variation rates of ESC and EDC, respectively. $a_{\mathrm{T}}^{\min}$ and $c_{\mathrm{T}}^{\min}$ separately represent the ESC and EDC of a specific rock type under the minimal confining pressure. For instance, $a_{\mathrm{T}}^{\min}$ of the RS tested is 0.8033, which corresponds to the 5 MPa confining pressure (Fig. 8(a)). Note that for a given rock type, the variation rate under the minimal confining pressure is 0. From Fig. 8, it appears that r_{a} is positive and r_{c} is negative (Figs. 8(a−d)). In most cases, the r_{a} increases and r_{c} decreases with increasing confining pressure. For example, the r_{a} of LS increases from 0 to 22.83% and related r_{c} varies from 0 to −32.04% when the confining pressure changes from 1 to 25 MPa (Fig. 8(c)). However, the SI and CM seem to exhibit opposite results compared with the remaining three rocks. This case may result from the difference in physical properties of specimens under the minimal confining pressure and other higher confining pressures, as mentioned previously. For all rock types, the influence of confining pressure on the ESC is less pronounced than that on the EDC. For example, when the confining pressure of CM changes from 2.5 to 10 MPa, the absolute maximum of r_{a} reaches 23.79% and the maximum r_{c} reaches 26.74%.

The ESC and EDC essentially reflect the distribution characteristics of strain energy during prepeak loading of rocks. Since these two coefficients are both formulated in ratio forms, they only characterize the rock energy storage and/or dissipation ability from a relative aspect. Figure 8(f) depicts proportions of U_i^{e} and U_i^{d} of five rock types subjected to different confining pressures. It is found that the distribution of pre-peak strain energy is not only influenced by the confining pressure, but also by the material property. For the CM, the proportion of U_i^{d} is clearly larger than that of U_i^{e}. Conversely, the other remaining four rock types exhibit the opposite energy proportions. Under a given confining pressure, U_i^{e} presents a larger proportion than U_i^{d}. In more details, for the tested LS, when the confining pressure varies from 1 to 25 MPa, the proportion of U_i^{e} increases from 58.39% to 71.72%, and the proportion of U_i^{d} decreases from 41.61% to 28.28%. For the RS, SI, and LS under the confining pressure of 10 MPa, the proportions of U_i^{e} are 80.476%, 71.36 %, and 60.79%, respectively, and the RS exhibits the maximum of U_i^{e} and the minimum of U_i^{d} among the five rock types.

4 Application of LES and LED laws

4.1 Prediction of peak strain energy under various confining pressures using LES law

The state of strain energy at peak strength (named as peak strain energy) has great importance for studying rock fracturing phenomena. Here, the LES law was used to predict the peak strain energies. The peak input strain energy (PISE) is directly computed by integrating the stress−strain curve, which is similar to the approach of obtaining the U_i^{I} at a given stress level in Fig. 2. Based on this, the related peak elastic strain energy (PESE) and peak dissipated strain energy (PDSE) can be deduced using Eq. (5). Figure 9 demonstrates PDSE, PESE and PISE in triaxial compression with different confining pressures. It is observed from Fig. 9 that under a constant confining pressure, the amount of PESE is apparently greater than that of the PDSE, reaching about four times. This implies that energy storage instead of energy dissipation dominates at the peak strength of rock. In addition, with an increase in confining pressure, the three peak strain energies all increase. This is because the existence of confinement improves the bearing limit of rock, thus comprehensively enhancing the ability of absorbing, storing, and dissipating the strain energy within the rock. As the confining pressure changes from 5 to 15 MPa, the PESE increases

from 0.1988 to 0.4763 mJ/mm^3, increased by 139.59%. The related PDSE varies from 0.0484 to 0.1059 mJ/mm^3, with a 118.80% increment. Since the PESE describes an absolute energy state at peak strength, it reflects the ultimate ability of rock to store strain energy. It can be confirmed that the confining pressure is instrumental in energy storage of rock from an absolute energy aspect.

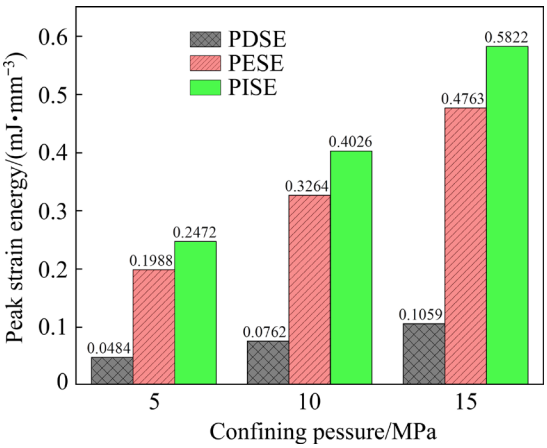

Fig. 9 Peak strain energies predicted using mutual linear relationships between pre-peak strain energies under different confining pressures

Table 2 lists the proportions of PESE and PDSE under different confining pressures, wherein the PISE is the sum of the associated PESE and PDSE. Under the confining pressures of 5, 10, and 15 MPa, the proportions of PESE are 80.41%, 81.08%, and 81.82%, and those of the PDSE are 19.59%, 18.92%, and 18.18%, respectively. This indicates that an increase in confining pressure improves the proportion of PESE and reduces the proportion of PDSE. This also signifies that the existence of confining pressure is more prone to promote the energy storage performance and weaken the energy dissipation capacity at rock peak strength. A higher confining pressure can more effectively curb the development and propagation of rock internal cracks and thus reduce the dissipation of strain energy.

4.2 Damage evolution analysis of triaxially compressed rock considering LED law

Rock will deform and be subject to damage under external loading due to the occurrence of micro cracks and permanent deformation. The investigation into rock damage has a great significance for the safety evaluation of deep rock engineering structures [44,45]. The theoretical investigations have indicated that rock damage is related to micro-failure, and that permanent failure can be characterized from the viewpoint of energy dissipation [46,47]. However, the damage evolution mechanism in rock under coupled conditions of confining pressure and cyclic loading still remains elusive [29]. In previous studies, a rock damage variable has been established based on energy dissipation. The damage variable is determined as the ratio of U_i^{d} to $U_{\mathrm{p}}^{\mathrm{d}}$ [44, 48]:

$$D = U_i^{\mathrm{d}} / U_{\mathrm{p}}^{\mathrm{d}} \tag{9}$$

where D is the damage variable, and $U_{\mathrm{p}}^{\mathrm{d}}$ denotes the peak dissipated strain energy. In essence, since the rock in triaxial cyclic compression obeys the LED law, D can be expressed as

$$D = \frac{U_i^{\mathrm{d}}}{U_{\mathrm{p}}^{\mathrm{d}}} = \frac{c_{\mathrm{T}} U_i^{\mathrm{I}}}{c_{\mathrm{T}} U_{\mathrm{p}}^{\mathrm{I}}} = \frac{U_i^{\mathrm{I}}}{U_{\mathrm{p}}^{\mathrm{I}}} \tag{10}$$

where $U_{\mathrm{p}}^{\mathrm{I}}$ represents the peak input strain energy.

Figure 10 describes the variations in damage variable with axial strain under triaxial cyclic compression conditions. The damage variable generally increases as the axial loading strain increases. In the initial loading stage, the damage variable increases slowly with the axial strain. When the axial strain is low, the damage variable of the same rock type subject to different confining pressures is nearly the same. However, when the axial strain becomes greater, with the same axial strain, the damage variable under a higher confining pressure is smaller than that under a lower confining pressure. Furthermore, for the same rock

Table 2 Amount and proportions of PESE and PDSE under different confining pressures

Confining pressure/MPa	PISE/ (mJ·mm^{-3})	PESE/ (mJ·mm^{-3})	PDSE/ (mJ·mm^{-3})	Proportion of PESE in PISE/%	Proportion of PDSE in PISE/%
5	0.2472	0.1988	0.0484	80.41	19.59
10	0.4026	0.3264	0.0762	81.08	18.92
15	0.5822	0.4763	0.1059	81.82	18.18

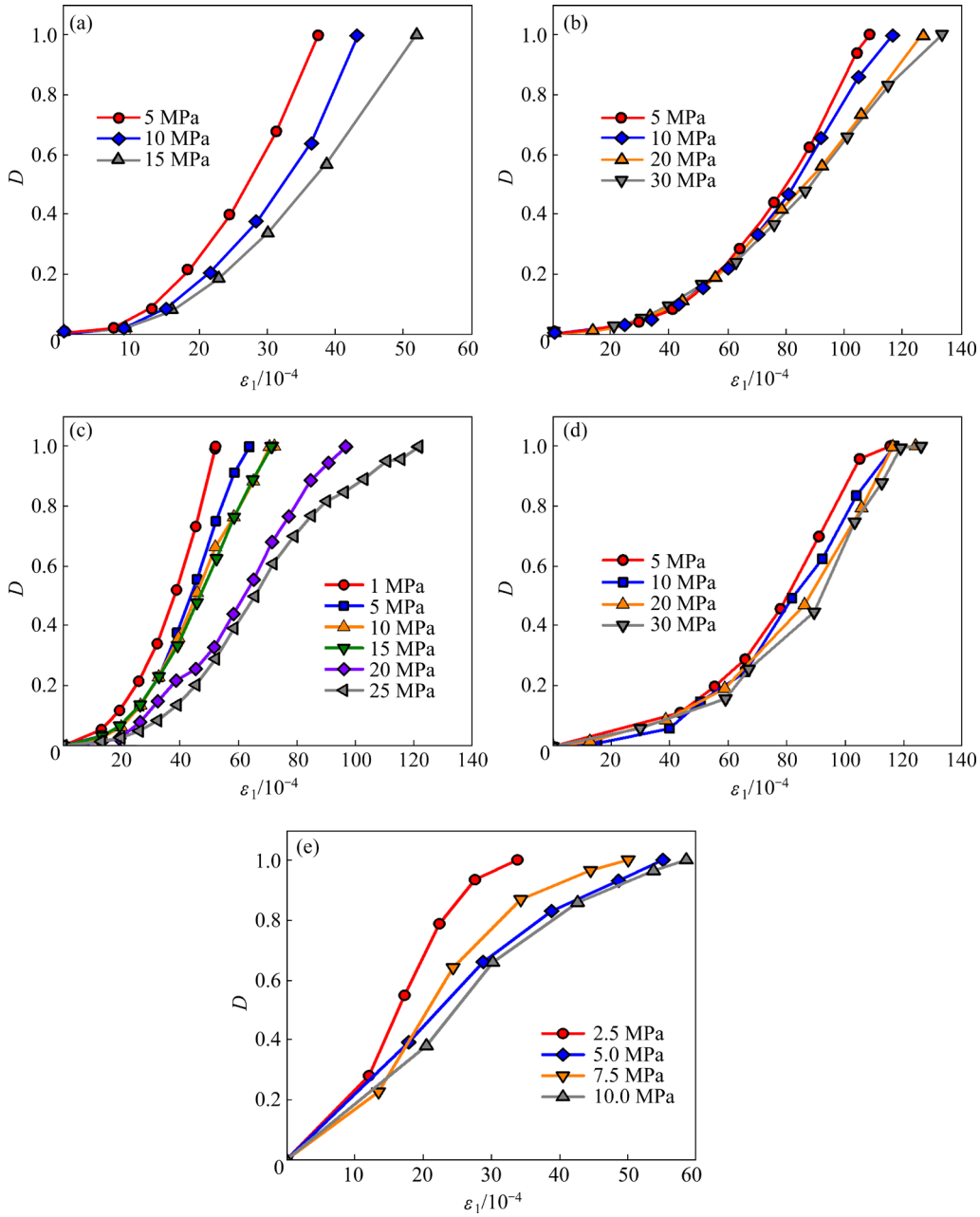

Fig. 10 Damage variable versus axial strain of rocks under triaxial cyclic compression with different confining pressures: (a) RS; (b) SI; (c) LS; (d) SII; (e) CM

type, as the confining pressure increases, the damage evolution gradually becomes gentler. This is because the higher confining pressure can more effectively inhibit the crack propagation during compression, thus reducing the damage of rocks.

5 Discussion

In this study, the LES and LED laws of rocks were revealed under triaxial cyclic compression conditions (a three-dimensional stress state). The universality of LES and LED laws of rocks in triaxial cyclic compression was also confirmed by analysing the experimental data in existing literature. Based on this, the revealed LES law was used to predict the peak strain energies of rocks. Considering the LED law, the damage evolution characteristics of rocks under various confining pressures were analyzed. In previous investigations, the LES and LED laws under one-dimensional and two-dimensional stress states have been reported [25,26,49]. Combined with the current work, these findings indicate that the LES and LED laws are applicable to rocks subjected to one-

dimensional to three-dimensional stress states. In addition, the LES and LED laws have been applied to the evaluation of rockburst proneness and the characterization of rock damage [4,24,44]. The above analysis shows that the LES and LED laws have a good application in related rock mechanics problems. However, the revealed LES and LED laws are limited to the pre-peak stage of rock deformation and failure. The energy law during rock post-peak failure is of great significance to the study of rock failure behavior, and the failure intensity of rocks is closely related to the energy state during post-peak stage. Whether there are LES and LED laws in the post-peak failure of rocks remains unclear. Therefore, the energy evolution laws of after-peak strength of rock are desired to be investigated in the future, and a wider experimental campaign for exploration may extend the related application of LES and LED laws.

6 Conclusions

(1) As the stress level increases, the elastic strain increases in linear relations, while the permanent strain follows U-shaped growth trend. Under a constant stress level, the higher the confining pressure is, the greater the elastic strain is.

(2) Under all confining pressures, the three pre-peak strain energies increase nonlinearly as the actual stress level increases. Importantly, the linear energy storage law and linear energy dissipation law of rocks in triaxial cyclic compression are further confirmed, and the universality of these linear energy laws is verified using the existing experimental results in literature. Through the linear energy storage law, the peak strain energies of rock under various confining pressures are predicted.

(3) The energy storage coefficient in triaxial compression is positively correlated to the confining pressure, while the corresponding energy dissipation coefficient shows opposite relations. From both the absolute and relative perspectives, it is shown that confining pressure can improve the energy storage performance of rocks.

(4) Based on the linear energy dissipation law, the damage evolution characteristics of rocks subjected to triaxial compression are analyzed. Under similar axial strain, the damage variable decreases as the confining pressure increases. This is because compared with low confinement, a higher confinement can restrain the generation and development of micro-cracks in rocks more effectively and thus reduce the rock damage degree.

Acknowledgments

This work was supported by the National Natural Science Foundation of China (No. 41877272) and the Fundamental Research Funds for the Central Universities, China (No. 2242022k30054).

References

[1] XIE He-ping, JU Yang, Li Li-yun. Criteria for strength and structural failure of rocks based on energy dissipation and energy release principles [J]. Chinese Journal of Rock Mechanics and Engineering, 2005, 24(17): 3003−3010. (in Chinese)

[2] ZHANG Zhi-zhen, GAO Feng. Confining pressure effect on rock energy [J]. Chinese Journal of Rock Mechanics and Engineering, 2015, 34(1): 1−11. (in Chinese)

[3] ZHAO Guo-yan, DAI Bing, DONG Long-jun, YANG Chen. Energy conversion of rocks in process of unloading confining pressure under different unloading paths [J]. Transactions of Nonferrous Metals Society of China, 2015, 25: 1626−1632.

[4] GONG Feng-qiang, LUO Song, JIANG Quan, XU Lei. Theoretical verification of the rationality of strain energy storage index as rockburst criterion based on linear energy storage law [J]. Journal of Rock Mechanics and Geotechnical Engineering, 2022, 14: 1737−1746. https://doi.org/10.1016/j.jrmge.2021.12.015.

[5] SI Xue-feng, HUANG Lin-qi, GONG Feng-qiang, LI Xi-bing. Failure process and characteristics of three dimensional high-stress circular tunnel under saturated water content [J]. Transactions of Nonferrous Metals Society of China, 2022, 32(8): 2696−2708.

[6] ZHANG Zi-zheng, DENG Ming, BAI Jian-biao, YU Xian-yang, WU Qiu-hong, JIANG Li-shuai. Strain energy evolution and conversion under triaxial unloading confining pressure tests due to gob-side entry retained [J]. International Journal of Rock Mechanics and Mining Sciences, 2020, 126: 104184.

[7] Si Xue-feng, HUANG Lin-qi, Li Xi-bing, Gong Feng-qiang, Liu Xi-ling. Mechanical properties and rockburst proneness of phyllite under uniaxial compression [J]. Transactions of Nonferrous Metals Society of China, 2021, 31: 3862−3878.

[8] WANG Shao-feng, TANG Yu, LI Xi-bing, DU Kun. Analyses and predictions of rock cuttabilities under different confining stresses and rock properties based on rock indentation tests by conical pick [J]. Transactions of Nonferrous Metals Society of China, 2021, 31: 1766−1783.

[9] ZHOU Xiao-ping. Triaxial compressive behavior of rock with mesoscopic heterogenous behavior: Strain energy density factor approach [J]. Theoretical and Applied Fracture Mechanics, 2006, 45: 46−63.

[10] HUANG Da, LI Yan-rong. Conversion of strain energy in triaxial unloading tests on marble [J]. International Journal of Rock Mechanics and Mining Sciences, 2014, 66: 160−168.

[11] PENG Rui-dong, JU Yang, WANG J G, XIE He-ping, GAO Feng, MAO Ling-tao. Energy dissipation and release during coal failure under conventional triaxial compression [J]. Rock Mechanics and Rock Engineering, 2015, 48: 509−526.

[12] MUNOZ H, TAHERI A, CHANDA E K. Fracture energy-based brittleness index development and brittleness quantification by pre-peak strength parameters in rock uniaxial compression [J]. Rock Mechanics and Rock Engineering, 2016, 49: 4587−4606.

[13] MUNOZ H, TAHERI A, CHANDA E K. Rock drilling performance evaluation by an energy dissipation based rock brittleness index [J]. Rock Mechanics and Rock Engineering, 2016, 49: 3343−3355.

[14] HE Ming-ming, HUANG Bing-qian, ZHU Cai-hui, CHEN Yun-sheng, LI Ning. Energy dissipation-based method for fatigue life prediction of rock salt [J]. Rock Mechanics and Rock Engineering, 2018, 51: 1447−1455.

[15] LI Ning, ZOU Yu-shi, ZHANG Shi-cheng, MA Xin-fang, ZHU Xing-wang, LI Sihai, CAO Tong. Rock brittleness evaluation based on energy dissipation under triaxial compression [J]. Journal of Petroleum Science and Engineering, 2019, 183: 106349.

[16] ZHANG Yan, FENG Xia-ting, ZHANG Xi-wei, WANG Zhao-feng, SHARIFZADEH M, YANG Cheng-xiang. A novel application of strain energy for fracturing process analysis of hard rock under true triaxial compression [J]. Rock Mechanics and Rock Engineering, 2019, 52: 4257−4272.

[17] ZHANG Yan, FENG Xia-ting, ZHANG Xi-wei, WANG Zhao-feng, SHARIFZADEH M, YANG Cheng-xiang, KONG Rui, ZHAO Jun. Strain energy evolution characteristics and mechanisms of hard rocks under true triaxial compression [J]. Engineering Geology, 2019, 260: 105222.

[18] ZHAO Hong-gang, SONG Zhen-long, ZHANG Dong-ming, LIU Chao, YU Bei-chen. True triaxial experimental study on mechanical characteristics and energy evolution of sandstone under various loading and unloading rates [J]. Geomechanics and Geophysics for Geo-Energy and Geo-Resources, 2021, 7: 22.

[19] GAO Fu-qing, YANG Lei. Experimental and numerical investigation on the role of energy transition in strainbursts [J]. Rock Mechanics and Rock Engineering, 2021, 54: 5057−5070.

[20] XIAO Wei-jing, YU Guo, LI Hai-tao, ZHAN Wei-yun, ZHANG Dong-ming. Experimental study on the failure process of sandstone subjected to cyclic loading and unloading after high temperature treatment [J]. Engineering Geology, 2021, 293: 106305.

[21] KHAN NM, MA Li-qiang, CAO Ke-wang, HUSSAIN S J, LIU Wei, XU Yu-jun, YUAN Qiu-peng, GU Jie. Prediction of an early failure point using infrared radiation characteristics and energy evolution for sandstone with different water contents [J]. Bulletin of Engineering Geology and the Environment, 2021, 80: 6913−6936.

[22] ZHANG Li-ming, CONG Yu, MENG Fan-zhen, WANG Zai-quan, ZHANG Peng, GAO Su. Energy evolution analysis and failure criteria for rock under different stress paths [J]. Acta Geotechnica, 2021, 16: 569−580.

[23] LIU Xiao-bo, ZHANG Zhen-yu, GE Zhao-long, ZHONG Chun-lin, LIU Li. Brittleness evaluation of saturated coal based on energy method from stress-strain curves of uniaxial compression [J]. Rock Mechanics and Rock Engineering, 2021, 54: 3193−3207.

[24] GONG Feng-qiang, YAN Jing-yi, Li Xi-bing. A new criterion of rock burst proneness based on the linear energy storage law and the residual elastic energy index [J]. Chinese Journal of Rock Mechanics and Engineering, 2018, 37(9): 1993−2014. (in Chinese)

[25] GONG Feng-qiang, YAN Jing-yi, LUO Song, LI Xi-bing. Investigation on the linear energy storage and dissipation laws of rock materials under uniaxial compression [J]. Rock Mechanics and Rock Engineering, 2019, 52: 4237−4255.

[26] LUO Song, GONG Feng-qiang. Linear energy storage and dissipation laws of rocks under preset angle shear conditions [J]. Rock Mechanics and Rock Engineering, 2020, 53: 3303−3323.

[27] GONG Feng-qiang, YAN Jing-yi, LI Xi-bing, LUO Song. A peak-strength strain energy storage index for rock burst proneness of rock materials [J]. International Journal of Rock Mechanics and Mining Sciences, 2019, 117: 76−89.

[28] JAFARI M K, PELLET F, BOULON M, HOSSEINI K A. Experimental study of mechanical behaviour of rock joints under cyclic loading [J]. Rock Mechanics and Rock Engineering, 2004, 37: 3–23.

[29] BAGDE M N, PETROS V. Fatigue properties of intact sandstone samples subjected to dynamic uniaxial cyclical loading [J]. International Journal of Rock Mechanics and Mining Sciences, 2005, 42(2): 237−250.

[30] SI Xue-feng, LI Xi-bing, GONG Feng-qiang, HUANG Lin-qi, LIU Xi-ling. Experimental investigation of failure process and characteristics in circular tunnels under different stress states and internal unloading conditions [J]. International Journal of Rock Mechanics and Mining Sciences, 2022, 154: 105116.

[31] DANG Wen-gang, KONLETZKY H, FRUHWIRT T, HERBST M. Cyclic frictional responses of planar joints under cyclic normal load conditions: Laboratory tests and numerical simulations [J]. Rock Mechanics and Rock Engineering, 2020, 53: 337–364.

[32] ZHOU Yong-qiang, SHENG Qian, LI Na-na, FU Xiao-dong, ZHANG Zhen-ping, GAO Li-song. A constitute model for rock materials subjected to triaxial cyclic compression [J]. Mechanics of Materials, 2020, 144: 103341.

[33] FARADONBEH R S, TAHERI A, KARAKUS M. Fatigue failure characteristics of sandstone under different confining pressures [J]. Rock Mechanics and Rock Engineering, 2022, 55: 1227–1252.

[34] YOU Wei, DAI Feng, LIU Yi, Yan Ze-lin. Effect of confining pressure and strain rate on mechanical behaviors and failure characteristics of sandstone containing a pre-existing flaw [J]. Rock Mechanics and Rock Engineering, 2022, 55: 2091–2109.

[35] YANG Sheng-qi, RANJITH P G, HUANG Yan-hua, YIN Peng-fei, JING Hong-wen, GUI Yi-lin, YU Qing-lei. Experimental investigation on mechanical damage characteristics of sandstone under triaxial cyclic loading [J].

Geophysical Journal International, 2015, 201(2): 662−682.
[36] CHEN Xu, TANG Ming-gao. TANG Chun-an. Effect of confining pressure on the damage evolution and failure behaviors of intact sandstone samples during cyclic disturbance [J]. Rock Mechanics and Rock Engineering, 2021, 55: 19−33.
[37] YANG Sheng-qi, YANG Jing, XU Peng. Analysis on pre-peak deformation and energy dissipation characteristics of sandstone under triaxial cyclic loading [J]. Geomechanics and Geophysics for Geo-Energy and Geo-Resources, 2020, 6: 24.
[38] MENG Qing-bin, LIU Jian-feng, HUANG Bing-xiang, PU Hai, WU Jiang-yu, ZHANG Zhi-zhen. Effects of confining pressure and temperature on the energy evolution of rocks under triaxial cyclic loading and unloading conditions [J]. Rock Mechanics and Rock Engineering, 2022, 55, 773−798.
[39] YANG Xiao-bin, CHENG Hong-ming, LÜ Jia-qi, HOU Xin, NIE Chao-gang. Energy consumption ratio evolution law of sandstones under triaxial cyclic loading [J]. Rock and Soil Mechanics, 2019, 10(10): 3751−3766. (in Chinese)
[40] MENG Qing-bin, WANG Cong-kai, HUANG Bing-xiang, PU Hai, ZHANG Zhi-zhen, SUN Wen, WANG Jie. Rock energy evolution and distribution law under triaxial cyclic loading and unloading conditions [J]. Chinese Journal of Rock Mechanics and Engineering, 2020, 39(10): 2047−2059. (in Chinese)
[41] MIAO Sheng-jun, LIU Ze-jing, ZHAO Xing-guang, HUANG Zheng-jun. Energy dissipation and damage characteristics of Beishan granite under cyclic loading and unloading [J]. Chinese Journal of Rock Mechanics and Engineering, 2021, 40(5): 928−938. (in Chinese)
[42] ZHOU Tian-bai, QIN Yue-ping, Ma Qiu-feng, LIU Jia. A constitutive model for rock based on energy dissipation and transformation principles [J]. Arabian Journal of Geosciences, 2019, 12(5): 492.
[43] YANG Sheng-qi, TIAN Wen-ling, RANJITH PG. Experimental investigation on deformation failure characteristics of crystalline marble under triaxial cyclic loading [J]. Rock Mechanics and Rock Engineering, 2017, 50: 2871–2889.
[44] GONG Feng-qiang, ZHANG Pei-lei, LUO Song, LI Jian-chun, HUANG Da. Theoretical damage characterization and damage evolution process of intact rocks based on linear energy dissipation law under uniaxial compression [J]. International Journal of Rock Mechanics and Mining Sciences, 2021, 146: 104858.
[45] CAO Ke-wang, MA Li-qiang, WU Yu, SPEARING A J S, KHAN N M, HUSSAIN S, REHMAN F U. Statistical damage model for dry and saturated rock under uniaxial loading based on infrared radiation for possible stress prediction [J]. Engineering Fracture Mechanics, 2022, 260: 108134.
[46] XU Lei, GONG Feng-qiang, LUO Song. Effects of pre-existing single crack angle on mechanical behaviors and energy storage characteristics of red sandstone under uniaxial compression [J]. Theoretical and Applied Fracture Mechanics, 2021, 113: 102933.
[47] LUO Song, GONG Feng-qiang. Linear energy storage and dissipation laws during rock fracture under three-point flexural loading [J]. Engineering Fracture Mechanics, 2020, 234: 107102.
[48] CHEN Zi-quan, HE Chuan, MA Gao-yu, XU Guo-wen, MA Chun-chi. Energy damage evolution mechanism of rock and its application to brittleness evaluation [J]. Rock Mechanics and Rock Engineering, 2019, 52: 1265−1274.
[49] SU You-qiang, GONG Feng-qiang, LUO Song, LIU Zhi-xiang. Experimental study on energy storage and dissipation characteristics of granite under two-dimensional compression with constant confining pressure. Journal of Central South University, 2021, 28: 848−865.

不同围压三轴循环压缩下岩石的线性储能和耗能规律及损伤演化特征

罗 松[1]，宫凤强[1,2]，李留留[1]，彭 康[1]

1. 中南大学 资源与安全工程学院，长沙 410083;
2. 东南大学 土木工程学院，南京 211189

摘 要：为了研究岩石的能量分布规律及其围压效应，开展不同围压下的三轴循环压缩试验。基于所得应力−应变曲线计算不同应力水平下的峰前输入应变能、峰前弹性应变能和峰前耗散应变能。结果表明，不同围压下峰前弹性应变能和峰前耗散应变能与峰前输入应变能呈明显线性相关，从而得到三轴循环压缩下的线性储能和耗能规律。岩石三轴压缩储能系数与围压呈正相关，而对应的耗能系数则相反。利用线性储能规律，可以推导出岩石在三轴压缩作用下的峰值弹性应变能和峰值耗散应变能。此外，基于线性耗能规律分析了不同围压下岩石的损伤演化特征。

关键词：能量分布规律；能量存储；能量耗散；三轴压缩；循环加载；围压

(Edited by Bing YANG)